A&A 567, A128 (2014)
DOI: 10.1051/0004-6361/201423579

Astronomy & Astrophysics

No X-rays from WASP-18

Implications for its age, activity, and the influence of its massive hot Jupiter⋆

Ignazio Pillitteri[1,2], Scott J. Wolk[2], Salvatore Sciortino[1], and Victoria Antoci[3]

[1] Osservatorio Astronomico di Palermo, Piazza del Parlamento 1, 90134 Palermo, Italy
e-mail: pilli@astropa.inaf.it
[2] SAO-Harvard Center for Astrophysics, 60 Garden St, Cambridge MA 02138, USA
[3] Stellar Astrophysics Centre, Department of Physics and Astronomy, Aarhus University, Ny Munkegade 120, 8000 Aarhus C, Denmark

Received 5 February 2014 / Accepted 10 June 2014

ABSTRACT

About 20% of the >1000 known exoplanets are Jupiter analogs orbiting very close to their parent stars. It is still under debate to what detectable level such hot Jupiters possibly affect the activity of the host stars through tidal or magnetic star–planet interaction. In this paper we report on an 87 ks *Chandra* observation of the hot Jupiter hosting star WASP-18. This system is composed of an F6 type star and a hot Jupiter of mass 10.4 $M_{\rm Jup}$ orbiting in less than 20 hr around the parent star. On the basis of an isochrone fitting, WASP-18 is thought to be 600 Myr old and within the range of uncertainty of 0.5–2 Gyr. The star is not detected in X-rays down to a luminosity limit of 4×10^{26} erg/s, which is more than two orders of magnitude lower than expected for a star of this age and mass. This value proves an unusual lack of activity for a star with an estimated age around 600 Myr. We argue that the massive planet can play a crucial role in disrupting the stellar magnetic dynamo created within its thin convective layers.
Other additional 212 X-ray sources are detected in the *Chandra* image. We list them and briefly discuss their nature.

Key words. stars: activity – stars: coronae – stars: individual: WASP-18

1. Introduction

About 20% of the >1000 extra solar planets discovered to date are hot Jupiters, meaning massive planets orbiting at a few stellar radii from the parent stars. Models predict that hot Jupiters could affect the activity of their host stars through either tidal or magneto-hydrodynamical interaction (e.g. Cuntz et al. 2000 and Ip et al. 2004). Both effects strongly scale with the separation d between the two bodies (Saar et al. 2004). Observational evidence of star-planet interaction (SPI) was first reported by Shkolnik et al. (2003), who discovered variability in the chromospheric activity indicators, the H and K lines of Ca II of HD 179949, phased with the planetary motion. Subsequently, Fares et al. (2010) have reconstructed the magnetic field of HD 179949 and confirm periodic variations of chromospheric activity indicators (Hα and Ca II lines) synchronized with the beat period of the planet-star system.

In the X-ray band, Kashyap et al. (2008) show that stars with hot Jupiters are statistically brighter by up to a factor four than stars with distant planets. Krejčová & Budaj (2012) support the findings of Kashyap et al. (2008) by means of a survey of Ca II H and K lines on planet hosting stars that traces a relationship betweeen stellar activity and planet-star separation, with closer hot Jupiters orbiting more active stars. However, Poppenhaeger et al. (2010) and Poppenhaeger & Schmitt (2011) argue that that the above results are biased by selection effects, and SPI is not a common phenomenon, but instead SPI only manifests itself in peculiar cases.

One of the clearest cases of detection of SPI is HD 189733. We have observed this system three times with *XMM-Newton* and found strong evidence of SPI at work in X-rays (Pillitteri et al. 2010, 2011, 2014). The first evidence comes from the overall activity of the host star. The very low level of X-ray activity of the M type companion, HD 189733B, puts a strong constraint on the age of the system at ≥2 Gyr (Pillitteri et al. 2010; Poppenhaeger et al. 2013). Supported also by the 2011 and 2012 *XMM-Newton* observations, the old age of HD 189733B is reinforced by the fact that it does not show flaring variability on a time scale of a few hours and within the *XMM-Newton* exposures (30−50 ks), as in young or active M-type stars. The old age of the secondary is inconsistent with the young age of the system as derived from stellar activity of HD 189733A, which is about 600 Myr (Melo et al. 2006). Schröter et al. (2011) report a similar result on CoRoT-2A. Based on *Chandra* observations of a planetary transit, they find that the primary is X-ray bright with a luminosity $\sim 1.9 \times 10^{29}$ erg s^{-1}, indicating an age <300 Myr, while a potential stellar companion of CoRoT-2A is undetected down to a limit of $L_{\rm X} \sim 9 \times 10^{26}$ ergs s^{-1}, implying a much older age.

In main sequence stars, coronal activity is tightly linked with the internal structure of the stars, because of the link between convective zone, dynamo action, and magnetic field emergence. Stellar activity is a handle for understanding the depth of the convective zone and the efficiency of the dynamo. In stars with intermediate masses, approximately from late A-type stars and

⋆ Full Table 2 is available in electronic form at http://www.aanda.org

Table 1. Main properties of the WASP-18 system.

Name	Type	Mass	Radius	Distance	$T_{\rm eff}$	V	Age
WASP-18	F6IV-V	$1.28 \pm 0.09\ M_{\odot}$	$1.29 \pm 0.16\ R_{\odot}$	100 ± 10 pc	6400 ± 75 K	9.3 mag	0.63 (0.5–2 Gyr)
Name	Type	Mass	Radius	Period	Semi-major axis	Note	
WASP-18b	hot Jupiter	$10.4 \pm 0.4\ M_{\rm Jup}$	$1.165 \pm 0.077\ R_{\rm Jup}$	$0.9414518 \pm 4 \times 10^{-7}$ d	0.0205 ± 0.0004 AU	Transiting	

Notes. Photospheric data from Doyle et al. (2013), other data from the catalog at exoplanet.eu. The range of age is from Southworth et al. (2009).

moving toward earlier types, the thin convective layer disappears, and so do magnetic dynamo and coronal emission. The precise onset of the convection is a function of the mass, the chemical composition, which affects the opacity of the inner layers of the star, and the stellar evolutionary stage. Mid F-type stars like our target, WASP-18, should possess a thin convective layer that can still generate an $\alpha - \omega$ dynamo similar to the solar one and produce a X-ray bright corona. In fact, mid and late F stars are X-ray bright in young clusters like the Hyades (600 Myr) at a level of $L_{\rm X} > 10^{28.5}$ erg/s. In the framework of the relationship between age, rotation, convective zone depth, dynamo, and coronal activity, the emission of X-rays in this range of masses is a probe of the dynamo efficiency from thin convective layer coupled with the rotation of the star. In late F-type stars with hot Jupiters at the age of Hyades, an enhancement of the X-ray activity should then be expected.

With the intent of exploring SPI as a function of the star-planet separation in a star with shallow convective zone, we observed the system of WASP-18 with *Chandra* for a whole orbital period of its planet. WASP-18 (HD 10069, 2MASS J01372503-4540404) is a F6 star at ∼100 pc from the Sun that harbors a very close-in hot Jupiter, with the planet orbiting in only 19.4 h (Hellier et al. 2009). The main characteristics of this system are given in Table 1 and are obtained from a recent spectroscopic study by Doyle et al. (2013). Numerous optical spectroscopic observations allowed quite precise estimates of the effective temperature, gravity, distance, chemical abundances and mass of WASP-18 (Doyle et al. 2013).

WASP-18b has a mass of about 10.43 $M_{\rm jup}$ and a density $\rho = 6.6\rho_{\rm Jup}$. Owing to a star-planet separation of only 3.48 R_* (0.02047 AU), the planet is experiencing strong irradiation that heats and bloats its atmosphere and fills its Roche lobe. Southworth et al. (2009) estimate an equilibrium temperature of about 2400 K. The close separation suggests that the planet is on the verge of the final spiralling phase toward the parent star and this gives an opportunity to observe the final phases of a planet before disruption (Brown et al. 2011).

While WASP-18 was known to have low activity based on the $\log R'_{\rm HK}$ indicator, the remarkably close separation between planet and star demands further studies of this system to explore the effects of SPI, both of tidal and magnetical origins. A star with an age of 600 Myr is expected to have a level of X-ray luminosity typical of that of Hyades ($L_{\rm X} \sim 10^{28.5}$–$10^{29.5}$ erg/s, Stern et al. 1995; Randich & Schmitt 1995). Despite this range of presumed X-ray luminosity, WASP-18 was undetected in a 50 ks stacked *Swift* exposure (Miller et al. 2012) at a limit of $\log L_{\rm X,lim} = 27.5$, and in the ROSAT All Sky Survey (which has a typical sensitivity of $\log f_{\rm X} \geq 10^{-12}$ erg s^{-1} cm^{-2}).

In this paper, we report the absence of detected X-ray emission from WASP-18 in a 87 ks deep *Chandra* exposure and its implications for the models of star-planet interaction and the evolutionary stage of this system. The structure of the paper is as follows. Section 2 describes the information on the age of WASP-18, Sect. 3 describes the observations and data analysis, and Sect. 4 reports our results. Finally, in Sects. 5 and 6 we discuss the results and draw our conclusions.

2. Age of WASP-18

With respect to our investigations the age of WASP-18 is a critical parameter, hence in this section. we discuss it in details. Estimating the age of a star is a difficult task, and best applied to a statistical sample like stars belonging to open clusters. Methods for dating the age of stars are semi- or fully empirical and rely on gyrochronology, rotation and activity tracers, or on isochrone fitting or asteroseismology, the last used especially for solar-like oscillators and red giants (Soderblom 2010). It is observed that stars during the main sequence phase lose angular momentum through magnetized stellar winds, so that for single stars it is possible to estimate their age from their rotation (Skumanich 1972).

Historically, activity tracers have been the Ca II H and K lines, Mg II H and K lines and Hα line (Wilson 1966; Vaughan & Preston 1980; Baliunas et al. 1995). All of them are sensitive to the chromospheric contribution to the line that is related to the overall stellar activity. Again, the connection between activity and rotation and between rotation and age makes measurement of these lines an empirical method for estimating the stellar age. However, in the cases of stars with hot Jupiters, the rotation and the activity tracers can be affected by the interaction with the planet, thus biasing the estimate of the age of the host star. Pillitteri et al. (2010, 2011, 2014); Poppenhaeger et al. (2013); Poppenhaeger & Wolk (2014) and Schröter et al. (2011) have found that the hot Jupiter hosting stars HD 189733 and CoRoT-2A have most likely been spun up by their close in planets, and thus their activity and rotation have been enhanced, thereby mimicking the behavior of younger stars. In HD 189733, activity tracers like X-ray luminosity would assign an age in the range 0.6–1.1 Gyr (Melo et al. 2006; Sanz-Forcada et al. 2011), while the stellar companion is much older. On the same star, Torres et al. (2008) used fitting to Y^2 isochrones (Demarque et al. 2004; Yi et al. 2001) to estimate an age of $\tau = 6.8^{+5.2}_{-4.4}$ Gyr.

The low chromospheric activity of WASP-18 would assign to it an age similar to that of the Sun or older. On the basis of isochrone fitting, the age of WASP-18 has been estimated by Hellier et al. (2009) and Southworth et al. (2009) to be similar to that of the Hyades but this estimate has a large range of uncertainty. Southworth et al. (2009) studied in details the stellar parameters of WASP-18 employing several models of stellar evolution: models from Claret and collaborators (Claret 2004, 2005, 2006, 2007), Y^2 models (Demarque et al. 2004; Yi et al. 2001), and *Cambridge* models (Eldridge & Tout 2004; Pols et al. 1998). The parameters from various models agree well with each other (less agreement is found for the results from *Cambridge* models), but overall the age of WASP-18 is found in the range from 0.5 to at most 2 Gyr. We assume this range of age for WASP-18 and in Sect. 4 we compare these values against the evidences of an older stellar age. For a star in

Table 2. List of X-ray sources detected in the ACIS image.

Num.	RA (J2000) deg	Dec (J2000) deg	Pos. err arcsec	Off-axis arcmin	Significance $\sigma_{\rm bkg}$	Counts cts	Cts err.	Rate ct ks^{-1}	Rate err.	Exp. time ks
1	24.23177	–45.54562	8.4	9.78	4.45	69.51	21.66	1.99	0.62	34.93
2	24.24039	–45.58173	2.5	7.77	4.13	18.18	7.29	0.296	0.119	61.37
3	24.24631	–45.52741	3.3	10.46	4.38	24.7	9.64	0.79	0.308	31.25
4	24.25307	–45.62677	1	5.41	9.44	30.27	9.06	0.399	0.119	75.95
5	24.26107	–45.64003	0.8	4.66	4.77	7.54	4.5	0.123	0.073	61.51
6	24.26128	–45.59062	1.9	6.83	4.2	13.33	5.74	0.183	0.079	72.66
7	24.26154	–45.59641	2.5	6.54	4.39	18.43	7.22	0.249	0.097	74.09
8	24.26997	–45.53962	2.2	9.4	12.45	76.95	11.65	1.359	0.206	56.61
9	24.27015	–45.62587	1.4	4.93	8.56	32.49	9.56	0.409	0.12	79.52
10	24.27129	–45.58701	2	6.79	7.52	35.92	10.77	0.487	0.146	73.81

Notes. Only ten rows are shown here. The full table is available online.

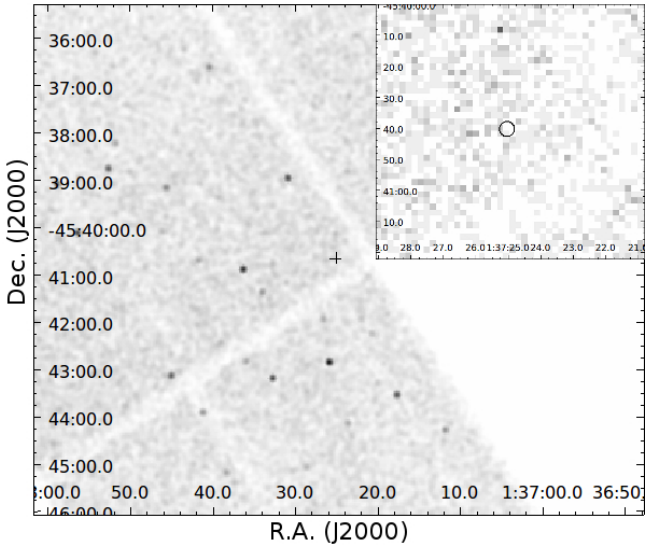

Fig. 1. *Chandra*-ACIS image toward WASP-18. The cross marks the position reported in the SIMBAD database. The *inset* image in the top right corner shows the region around the star, with the circle marking the position of WASP-18.

the 0.5–2 Gyr age time interval, corresponding to an age between that of the Hyades and of stars in NGC 752 open cluster, the X-ray luminosity of late F stars should be approximately in the range $28.1 < \log L_{\rm X} < 29.5$ (Pallavicini et al. 1981; Stern et al. 1995; Randich & Schmitt 1995; Giardino et al. 2007).

3. Observation and data analysis

We observed WASP-18 ($\alpha = 1^{\rm h}37^{\rm m}24.2^{\rm s}$, $\delta = -45^{\rm d}40^{\rm m}40.3^{\rm s}$, J2000) using *Chandra* with a continuous ~87 ks long observation with ACIS camera. ACIS CCDs number 1, 2, 3, 6, 7 were used. WASP-18 falls in the CCD nr. 3 (see Fig. 1). The star is not visible in the X-ray image and is not detected at a significance threshold of 4σ of local background, after applying a wavelet detection algorithm (Damiani et al. 1997b,a, 2003). The significance threshold of 4σ is the value usually adopted to statistically have at most one spurious source per field. We also ran the detection algorithm at a significance threshold of 3σ, but still no sources are found within 5″ from the nominal position of the star. We tested the hypothesis that WASP-18 could be heavily embedded in the material stripped from the outer atmosphere of the planetary companion. In this case the gas absorption should attenuate the soft part of the spectrum ($kT < 1$ keV), leaving any hard component spectrum still detectable. For this purpose we applied the same source detection procedure on the image in the 1.5–5.0 keV band without successful detection of any source at the position of WASP-18. Hence we exclude that WASP-18 is shrouded in X-rays by a dense gas layer from its hot Jupiter. At this point, we calculated an upper limit to the rate in 0.3–8.0 keV consistent with the 3σ threshold, and this value is 3.8×10^{-5} counts s^{-1}.

Table 2 reports the positions, offaxis, significance, counts, count rates, and exposure times of 212 detected sources detected above the 4σ threshold. We cross-correlated the positions of the detected sources against NED, 2MASS and Simbad catalogs in order to identify optical and IR counterparts. Table 4 reports the list of matches with notes about their nature. For the brightest sources, we also extracted the spectra, and performed a best fit, adopting either an absorbed thermal model or an absorbed power law with XSPEC software ver. 12.8. Table 5 lists the best fit parameters.

We obtained an archival FEROS spectrum of WASP-18 acquired on Sept. 9, 2010; in particular, we examinated the portion of spectrum around the H_α and the Li doublet (6708 Å). We estimated the rotational period of WASP-18 by deriving the projected rotational velocity v sin *i*. We measured the Gaussian full width at half maximum (FWHM) of the weak Fe lines around Li doublet equal to $FWHM = 0.42$ Å. We corrected this value by quadratically subtracting: a) 0.14Å of instrumental resolution; b) 1 km s^{-1} of micro turbulence; and c) 4 km s^{-1} of macro turbulence. The values of micro and macro turbulence are broadly consistent with those used by Doyle et al. (2013). We assumed that the axis of the planetary orbit aligned with the stellar rotational axis and an angle between orbital plane and line of sight $i = 86 \pm 2.5$ deg to obtain a value of rotational velocity $v \sim 17.2 \pm 0.5$ km s^{-1}. Given a stellar radius of 1.29 $R_\odot$, the rotational period is 3.7–3.9 days, which makes WASP-18 a moderate rotator. However, Doyle et al. (2013) report a slower v sin i (10.9 ± 0.7 km s^{-1}), which would give a period of $P \sim 6$ days. The discrepancy of our period (3.7–3.9 d) and the one inferred by Doyle et al. (2013) does not produce disagreement in the expected activity of WASP-18. For a star of the mass of WASP-18 and rotating in about four to six days, the expected X-ray luminosity should be $L_{\rm X} \geq 10^{29}$ erg s^{-1} (see Figs. 5 and 8 in Pizzolato et al. 2003).

4. Results

4.1. No X-rays from WASP-18

As stated in Sect. 2, WASP-18 is not detected in X-rays. The limiting count rate is $r_{\rm lim} = 3.8 \times 10^{-5}$ ct s^{-1}. By using PIMMS

software, we can estimate a limiting flux and luminosity from the upper limit to the rate. We assumed a thermal spectrum with one temperature at $kT = 0.5$ keV, analogous to HD 189733 and the plasma temperatures typical of young Hyades, and a gas absorption equal to $N_H = 1.5 \times 10^{20}$ cm^{-2}. We obtained a limit unabsorbed flux of 3.8×10^{-16} erg s^{-1} cm^{-2} in 0.3–8.0 keV band, which corresponds to a luminosity of $L_X \leq 4.5 \times 10^{26}$ erg s^{-1} at a distance of 100 pc. When using a softer spectrum ($kT = 0.3$ keV), the limiting flux and luminosity would be $f_X = 5.9 \times 10^{-16}$ erg s^{-1} cm^{-2} and $L_X = 1.5 \times 10^{27}$ erg s^{-1}, respectively. The L_X value are surprisingly low for a star whose age is estimated to be around 600 Myr like the Hyades. Late F stars in Hyades have a median luminosity of $L_X = 10^{29}$ erg s^{-1} with a dispersion of about 0.5 dex (Randich et al. 1998; Stern et al. 1995; Randich & Schmitt 1995).

Even older F type stars can emit more X-ray luminosity than WASP-18. For comparison, we report the serendipitous detection in X-rays of the F6V type star HD 110450, in a 20ks exposure devoted to observe R Mus (P.I. N. Remage Evans, Pillitteri et al. in prep). HD 110450 is very similar to WASP-18: it is at ∼100 pc from the Sun and has an age estimated between 2.1 Gyr and 3.9 Gyr (Casagrande et al. 2011; Holmberg et al. 2009). In X-rays, it has a PN rate of 20 ct/ks in the 0.3–8.0 keV band and the best fit to the spectrum gives a temperature of $kT = 0.2$ keV and $N_H = 3 \times 10^{21}$ cm^{-2}, unabsorbed flux of $f_X = 2.5 \times 10^{-13}$ erg s^{-1} cm^{-2}, and luminosity $L_X = 3.1 \times 10^{29}$ erg s^{-1}. From this comparison, we conclude that if WASP-18 has the same age as of HD 110450, its low X-ray activity would still be at odds with that of a typical F-type star. The inactive F5 type star Procyon and the F7 type hot-Jupiter host τ Boo have X-ray luminosities of $\log L_X \sim 28$ and $\log L_X = 28.8$ respectively. More interestingly, WASP-18 and τ Boo have similar rotational periods, 3.7–6 days for WASP-18, and 3.1–3.7 days for τ Boo (Catala et al. 2007). A similar level of X-ray activity should be observed because of the link between rotation and X-ray activity (Pallavicini et al. 1981; Pizzolato et al. 2003). However, the age of τ Boo is estimated to be around 2 Gyr, and its activity is perhaps boosted by magnetic SPI (Walker et al. 2008). WASP-18 stands out of the typical activity of similar mass stars.

Summarizing, WASP-18 is more than 2.5 orders of magnitude less luminous than Hyades, and about 2 orders of magnitude less active than the twin HD 110450, the inactive Procyon, and the similar planet host τ Boo. The absence of X-ray activity in WASP-18 agrees with the very low chromospheric activity reported by Knutson et al. (2010) and Miller et al. (2012), who report the non detection of this star in a 50 ks stacked *Swift* exposure at $\log L_{Xlim} = 27.5$. Its low activity would suggest a much older age, of a few Gyr, because of the relationship between activity-rotation and age in main sequence stars, hence an age comparable to that of the Sun or older. Nevertheless, the isochronal age estimate of WASP-18 appears plausible given the agreement of several stellar models (Southworth et al. 2009). At odds with an age older than 2 Gyr is also the moderately high rotational rate of WASP-18. The contradictory age estimates of WASP-18 imply that even an old age alone cannot explain the darkness of WASP-18 in X-rays. This points out to a role played by its close massive hot Jupiter.

5. Discussion

The first unexpected result we obtained with the 87 ks *Chandra* exposure is the very low upper limit to the X-ray luminosity of WASP-18 ($L_{Xlim} = 4.5 \times 10^{26}$ erg/s. The lack of X-ray and chromospheric activity of WASP-18 is inconsistent with its young age. Indeed the comparison with Hyades and with the similar stars, such as HD 110450, τ Boo, and Procyon, points to a much older age than given by Hellier et al. (2009). Optical spectra obtained at ESO Telescope with the FEROS spectrograph corfirm absence of activity and suggest an age similar to or older than that of the Sun (Soderblom 2010). Figure 2 shows the portion of one of the FEROS spectra around Hα. The line is seen completely in absorption, with no signs of filling-in of the core that could be due to chromospheric activity. Moreover, the many weak absorption lines of Fe and other metals are quite narrow meaning a slow stellar rotation. Altogether, these features demonstrate the low activity of WASP-18 and would suggest an age closer to the Sun's. Using the empirical calibration given by Soderblom (2010), despite its limitations, and the value of $\log R'_{HK} = -5.43$ reported by Knutson et al. (2010) gives us an age $\tau \geq 2.7$ Gyr. The chromospheric activity indicator of WASP-18 is even below the average value of cluster M 67 (4.5 Gyr, Soderblom 2010) and the solar value.

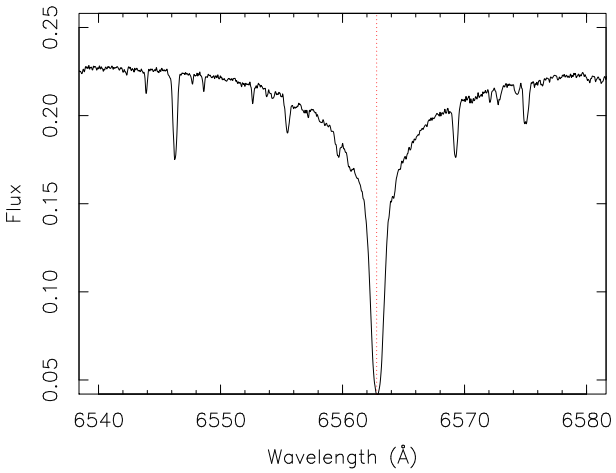

Fig. 2. Portion of FEROS spectrum of WASP-18 around Hα from the ESO archive of pipeline reduced spectra. This particular spectrum was taken on 19 Sept. 2010. We use arbitrary units for flux on the Y axis. Absence of core emission in Hα, and narrow lines support the idea that the star is not as young as Hyades and is a moderately high rotator.

However, the scenario becomes more puzzling when considering that WASP-18 shows Li absorption at 6708 Å, with a value typical of, or even stronger than values found in F-late stars of Hyades (Takeda et al. 2013) and M 67 (Pace et al. 2012). Figure 3 shows a portion of the spectrum of WASP-18 around the Li doublet lines at 6708 Å, and Fig. 4 shows the Li equivalent widths (EWs) vs. T_{eff} given by Pace et al. (2012) and Takeda et al. (2013) for Hyades and the older M 67 cluster. For comparison we show the FEROS spectrum of τ Boo, which has no Li absorption. The Li absorption in WASP-18 suggests a younger age with respect to τ Boo or a different efficiency in the mixing mechanism among these two stars of similar effective temperatures and masses. In WASP-18 the equivalent width (EW) that we measured is $EW(Li) = 46 \pm 2$ mÅ.

Compared to the values reported by Takeda et al. (2013) and Pace et al. (2012), WASP-18 has a slightly higher Li abundance. Lithium depletion is due to the convective mixing during the main sequence life of a star, so Li abundance is a rough indicator of youth in solar type stars with deep convective zone. In more massive stars, the mixing is less effective in bringing Li at the burning temperatures (2.5×10^6 K). However, in mid

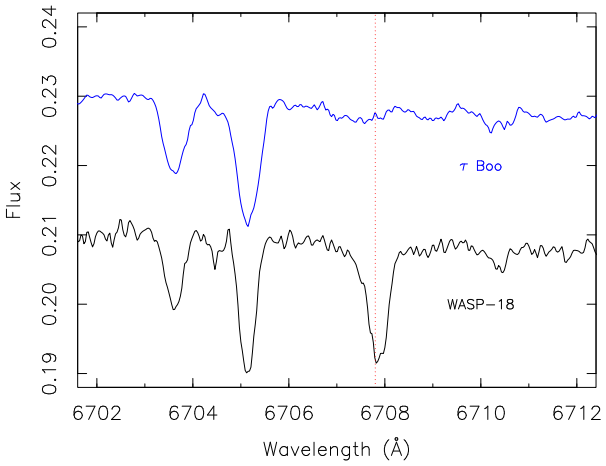

Fig. 3. Portion of the FEROS spectrum of WASP-18 around Li doublet at 6707.8 Å. This particular spectrum was taken on 19 Sept. 2010. We use arbitrary units for flux on Y axis. For comparison we also plot the FEROS spectrum of τ Boo in the same spectral range. The spectrum of τ Boo has been scaled and shifted in wavelength by +0.42 Å (accounting for its radial velocity) for an easier comparison with WASP-18. The Li feature is strong in WASP-18 and absent in τ Boo.

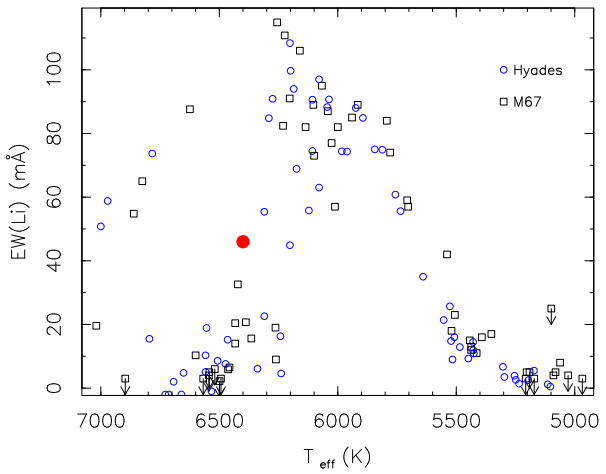

Fig. 4. EWs of Li vs. $T_{\rm eff}$ for Hyades (open squares), M 67 (open circles) and WASP-18 (filled circle). The EW(Li) of WASP-18 is EW = 46 ± 2 mÅ and suggests a young age like Hyades, contradicting the absent activity of its corona and chromosphere.

F type stars Li abundance shows a significant dip that has still not been understood. The dip appears between 6700 K and 6200 K (see Fig. 3), with a steep edge on the hot side and a slower rise on the cool side. WASP-18 is in this range of temperatures ($T_{\rm eff}$ ∼ 6400 K) and should have a low Li abundance.

Israelian et al. (2004) claim that stars harboring hot Jupiters have lower Li abundance than single stars, and similar results were reported by Gonzalez (2008) and Delgado Mena et al. (2014). Bouvier (2008) qualitatively explains this result by tracing it back to the pre main Sequence (PMS) history of the angular momentum of the star+disk system. A long-lived circumstellar disk during PMS creates a slow stellar rotator with a strong shear at the base of the convective zone and a more efficient mixing that accelerates the Li burning. At the same time, a long-lived disk offers more favorable conditions for the formation and the migration of exoplanets. WASP-18 has a significant Li abundance conflicting with the general pattern of Li in stars hosting hot Jupiters.

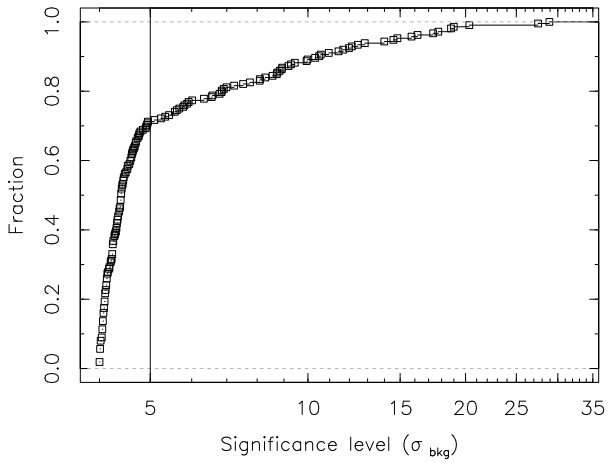

Fig. 5. Cumulative distribution of significance in $\sigma_{\rm bkg}$. Scale on x-axis is logarithmic. A break at a significance level $\sigma = 5$ is noticed.

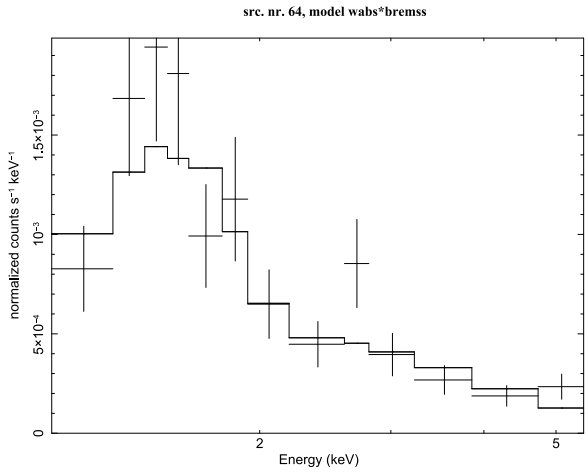

Fig. 6. X-ray spectrum and best fit model of src. 64. A line at ∼2.5 keV is noticed.

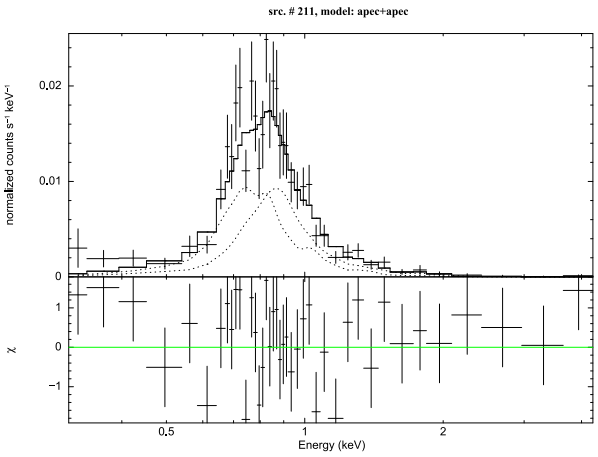

Fig. 7. X-ray spectrum and best fit model of the G8III/IV star HD 10210 (src. 211). A thermal model with two components (kT_1 = 0.37 keV, $KT_2 = 0,75$) is the best fit to the spectrum.

How can one reconcile the X-ray darkness, the absence of activity, an old age, and the "high" Li abundance in WASP-18? The solution to conflicting evidence could rely in the strong tidal interaction between the massive planet and its host star. We speculate that the tidal interaction in WASP-18 could interfere in

Table 3. Properties of stars with hot Jupiter s with T_{eff} in the range 6200−6600 K.

Star	$T_{\rm eff}$ K	$R_{\rm star}$ $R_\odot$	$M_{\rm star}$ $M_\odot$	$M_{\rm planet}$ $M_{\rm Jup}$	Separation AU	$\log R'_{\rm HK}$	H_P km	$H_{\rm t}$ km	$H_{\rm t}/H_P$
WASP-18	6400	1.29	1.28	10.43	0.02047	–5.43	419	498.3	1.189
WASP-12	6300	1.599	1.35	1.404	0.02293	–5.5	600.1	122.3	0.204
WASP-14	6475	1.306	1.211	7.341	0.036	–4.923	458.7	44	0.096
XO-3	6429	1.377	1.213	11.79	0.0454	–4.595	505.5	39.4	0.078
HAT-P-7	6350	1.84	1.47	1.8	0.0379	–5.018	735.5	37.2	0.051
HAT-P-2	6290	1.64	1.36	8.74	0.0674	–4.78	625.6	14.6	0.023
Kepler-5	6297	1.793	1.374	2.114	0.05064	–5.037	740.9	14.1	0.019
HAT-P-14	6600	1.468	1.386	2.2	0.0594	–4.855	516	3.4	0.007
HAT-P-6	6570	1.46	1.29	1.057	0.05235	–4.799	545.9	2.6	0.005
Kepler-8	6213	1.486	1.213	0.603	0.0483	–5.05	568.8	2.3	0.004
WASP-17	6650	1.38	1.2	0.486	0.0515	–5.331	530.7	1.1	0.002
HAT-P-9	6350	1.32	1.28	0.67	0.053	–5.092	434.7	1	0.002
WASP-19	5500	1.004	0.904	1.114	0.01616	–4.66	308.5	55.2	0.179

Notes. We list the effective temperatures, stellar masses and radii, planet-star separations, chromospheric activity indicator $\log R'_{HK}$ (from Knutson et al. 2010), pressure scale heights (H_P), tidal heights (H_t), and ratio H_t/H_P based on the formulae given by Cuntz et al. (2000). Stellar data are taken from the exoplanets.eu catalog and ordered by decreasing H_t/H_P ratio. Data of WASP-19 are shown because of the planet-star separation very similar to WASP-18. WASP-18 is the only star with pressure scale height and tidal height of the same order of magnitude. The second highest H_t/H_P ratio (∼ 20%) is seen in WASP-12, which has low activity like WASP-18.

Table 4. Optical and IR counterparts of X-ray sources.

#	RA (deg) X-ray pos.	Dec (deg) X-ray pos.	No.	NED name	RA(deg)	DEC(deg)	Type	Magnitude and filter	Separation arcsec
20	24.29519	–45.57693	62	APMUKS(BJ) B013505.04-454952.2	24.29543	–45.57682	G	18.99	0.7
22	24.3018	–45.60976	30	MRSS 244-010213	24.30153	–45.60971	G	18.9r	0.7
129	24.35544	–45.66886	6	APMUKS(BJ) B013519.66-455523.1	24.3557	–45.66886	G	20.29	0.7
131	24.3612	–45.67118	5	APMUKS(BJ) B013520.98-455532.3	24.36116	–45.67142	G	19.67	0.9
184	24.49494	–45.65133	49	MRSS 244-008106	24.49512	–45.65108	G	18.0r	1.0
186	24.50386	–45.75107	70	APMUKS(BJ) B013555.40-460017.6	24.5036	–45.75096	G	19.55	0.8

#	RA	Dec	RAJ2000	DEJ2000	2MASS name	Jmag	e_Jmag	Hmag	e_Hmag	Kmag	e_Kmag	Qflg	Sep.
20	24.29519	–45.57693	24.295321	–45.577065	01371087-4534374	16.6	0.14	15.9	0.13	15.2	0.16	BBC	0.6
184	24.49494	–45.65133	24.494989	–45.65136	01375879-4539048	16.74	0.154	15.80	0.15	15.0	0.13	BBB	0.2

#	RA	DEC	Simbad ID	OTYPE	pmRA	pmDEC	Plx_VALUE	Z_VALUE	B	V	SP_TYPE	Sep.
211	24.743367	–45.774851	HD 10210	Star	48.35	–1.45	6.33	4.8E-5	9.02	8.08	G8III/IV	1.6

Notes. The first part of the table lists the six NED counterparts, the second part lists the two 2MASS counterparts, the third part lists the only SIMBAD counterpart.

a significant way with the upper layers of the convective zone to the point of canceling out the magnetic activity and of reducing the mixing of the stellar material. Following Cuntz et al. (2000), we estimated a height of the tide of $H_{\rm t}$ ∼ 498 km. This value could still be a small fraction of the depth of the convective zone (∼16% R_*, Houdek et al. 1999; Trampedach et al. 2013). However, the depths of the convective zone in stars of mass of WASP-18 or higher are very sensitive to the mass and temperature, and in this range of temperatures its calculation suffers of significant uncertainties (see Claret 2004). Among a sample of exoplanet host stars with similar effective temperatures, WASP-18 has the highest ratio between tide height and pressure scale height (H_t/H_P). This ratio is on the order of 1.2 as shown in Table 3, where we list the ratios $H_{\rm t}/H_P$ of a sample of stars with hot Jupiters with effective temperatures $T_{\rm eff}$ in the range 6200−6600 K taken from Knutson et al. (2010). The $H_{\rm t}/H_P$ ratio takes into account the tidal effect due to the mass of the planet, its distance from the star (through $H_{\rm t}$), and the properties of the star ($T_{\rm eff}$, stellar mass and radius through H_P). We speculate that the tides on the stellar surface could influence the convective motions and the meridional circulation inside the convective layers to effectively reduce or nullify the mechanism of magnetic dynamo. The $H_{\rm t}/H_P$ ratio could be an empirical parameter of the efficiency of the planetary tide in reducing the shear within convective layers. The difference of Li in WASP-18 and τ Boo could be a manifestation of different tidal interactions in these two systems. It has been observed that in tidally locked binaries of Hyades, Li is more abundant than in single stars pointing to a role of tidal influence on the inner mixing of these stars (Thorburn et al. 1993; Deliyannis et al. 1994).

The existence of WASP-18b poses a strong constraint on the models of the dynamics of planets migrating inward. If the stellar age is in the range 2–4 Gyr, the inward planet migration has acted on a time scale of a few Gyr, not on a time scale of hundreds of Myr as derived by Brown et al. (2011). The orbital evolution of WASP-18 b has thus been slower than predicted by models of the orbital evolution of hot Jupiters. The low activity of the star also has consequences for the photo-evaporation of the planet and its lifetime. An X-ray and UV flux that is two orders of magnitude weaker than in other systems such as τ Boo and HD 189733, produces much less evaporation of the upper layers of the planetary atmosphere, making the process slower than in other active hosts of hot Jupiters (Penz & Micela 2008; Sanz-Forcada et al. 2011). We expect that Roche-Lobe

Table 5. Best fit models and parameters.

#	Model name	χ^2	d.o.f.	N_H	err(N_H)	kT/α	err(KT/α)	Norm	err(Norm)			Flux
				cm^{-2}		keV/–		cm^{-5}				erg s^{-1} cm^{-2}
8	Abs+Pow	2.82	6	0.10	0.22	1.8	0.5	4.2e-06	2.0e-06			2.0e-14
20	Abs+Pow	4.13	4	0.35	0.50	0.51	0.5	1.8e-06	1.3e-06			4.0e-14
22	Abs+Pow	4.13	4	0.35	0.5	0.5	0.5	1.8e-6	1.2e-6			5.4e-14
57	Abs+Pow	9.7	5	0.4	0.3	3.5	0.8	1.7e-05	1.0e-05			1.7e-14
64	Abs+Brems	13.0	10	0.61	0.27	4.9	2.9	1.33e-05	4.1e-06			3.5e-14
90	Abs+Pow	6.91	3	4.6	1.9	2.9	1.0	4.3e-05	5.8e-05			1.8e-14
104	Abs+Pow	4.51	6	0.13	0.16	1.9	0.4	5.5e-06	2.1e-06			2.2e-14
135	Abs+Pow	0.45	1	1.2	0.8	2.1	0.8	4.4e-06	4.8e-06			9.6e-15
145	Abs+Pow	0.96	1	0.02	0.20	1.8	0.5	1.6e-06	0.9e-06			9.0e-15
182	Abs+Pow	2.35	2	0.0	0.2	1.6	0.5	1.7e-06	0.9e-06			1.2e-14
190	Abs+Pow	0.22	3	0.0	0.23	1.5	0.5	4.3e-06	2.3e-06			3.1e-14
#	Model	χ^2	d.o.f.	kT_1	err(KT_1)	kT_2	err(KT_2)	Norm1	err(Norm1)	Norm2	err(Norm2)	flux
211	Apec+Apec	41.1	36	0.37	0.06	0.75	0.1	4.1e-5	2.0e-5	2.7e-5	1.7e-5	9.1e-14

Notes. We used an absorbed power law as model (Abs+Pow) for all but two cases, where we used absorbed bremsstrahlung (src. # 64, Abs+Brems) and two thermal models (src. # 211, Apec+Apec). Errors are given at the 1σ level.

enhancement of the evaporation (Erkaev et al. 2007) should not be important in WASP-18b, given its mass (~10.4 M_{jup}).

The absence of a significant corona explains why the star is dark in X-rays. WASP-18 demonstrates that SPI of tidal and magnetic origin must depend on both stellar structure and evolutionary stage. A different example of SPI in a star with a very close-in hot Jupiter is given by WASP-19. Like WASP-18, WASP-19 has a close-in hot Jupiter that orbits in less than one day. However, WASP-19 is a K type star with a deep convective zone and has a planet of almost the mass of Jupiter. WASP-19 shows high chromospheric emission, at a level similar to HD 189733 (Knutson et al. 2010). The H_t/H_P ratio in WASP-19 is 18% and the height of the tide is 55.2 km, a very small fraction of the depth of the convective zone in this star. We argue that the different stellar structures of WASP-19 and WASP-18 probably result in different dynamo strengths and coronal emission. We argue that in the case of WASP-19, the tidal interaction cannot significantly affect the motions of material inside the convective zone as in the case of WASP-18. As a consequence, a magnetic dynamo can still be established, and magnetic SPI is at work in this system enhancing the overall activity of WASP-19. With opposite effects, the tidal interaction of WASP-18b takes over the magnetic influence and suppresses the magnetic dynamo of WASP-18.

In summary, the factors that lead to SPI not only are a function of planet-star separation and planet/star mass ratio, but also rely on the inner structure of the parent star, the efficiency of its dynamo, its age, and the strength of a planetary magnetic field.

6. Summary and conclusions

With the aim of detecting the effects of star-planet interaction at high energies, we analysed a 87 ks deep *Chandra* observation pointed toward the star with hot Jupiter WASP-18. We do not find any X-ray emission from the star at a level above $L_X = 4.5 \times 10^{26}$ erg s^{-1}. The star is at least 2.5 orders of magnitude less luminous in X-rays than analog F late stars in Hyades, and main sequence stars like τ Boo, the 4 Gyr old star HD 110450 and Procyon, which is at the very end of the main sequence or already post main sequence. The absence of X-ray activity agrees with the low chromospheric activity reported by Knutson et al. (2010), with the absence of reversal core emission in the Hα and Ca H and K lines. These facts strongly conflict with the estimate of the age from fitting to isochrones (600 Myr) given by Hellier et al. (2009) and Southworth et al. (2009), and with the strong Li absorption observed in optical spectra and would suggest an activity level that is more consistent with a solar age.

A stellar age of a few Gyr puts strong constraints on the evolution model of the planet. In particular, it implies that the inward planet migration took place on a time scale of a few Gyr, not on a time scale of hundreds of Myr as assessed by Brown et al. (2011). The orbital evolution of WASP-18 b may therefore have been slower than predicted by models.

The absence of X-ray activity in the star also indicates a null efficiency of the magnetic dynamo. In these conditions, magnetic SPI is not at work, but rather, a strong tidal influence from the massive hot Jupiter can play a major role in determining the outer stellar structure and activity of WASP-18. To reconcile the strong Li absorption with an absent activity, we suggest a scenario in which the tidal interaction of the massive planet has modified the inner stellar mixing, thus preventing or at least reducing the Li burning. At the same time, the upper layers of the thin convective zone expected at this stellar mass are profoundly altered by tidal stresses. In a sample of stars with hot Jupiters in the same range of effective temperature, WASP-18 is the only object to show a tide height, induced by its planet, that is higher than the gas pressure scale height. The motions induced by tidal SPI could reduce the shear within the convective zone, hampering the creation of a magnetic dynamo and thus the outer corona and the production of X-rays. The same tides could be responsible for reducting the mixing efficiency in the inner stellar layers resulting in a higher Li abundance than observed in stars of similar mass, like τ Boo. This hypothesis requires detailed simulations in the framework of two-body interaction and modification of the stellar structure in binary systems. Our results can be a stimulus to understanding any of these effects, and then highlight the uniqueness of WASP-18 among systems with hot Jupiters.

We find 212 X-ray sources in the ACIS image. We briefly discuss their characteristics in the Appendix.

Acknowledgements. I.P. and S.J.W. are grateful to Dr. S. Saar for his comments on this paper. I.P. acknowledges financial support from the European Union under the project "Astronomy Fellowships in Italy" (AstroFit). S.J.W. was supported by NASA contract NAS8-03060. V.A. is grateful to Dr. R. Trampedach for the discussion about the models of stellar convection. V.A. acknowledges funding for the Stellar Astrophysics Centre provided by The Danish National Research Foundation; the research is supported by the ASTERISK project (ASTERoseismic Investigations with SONG and *Kepler*) funded by the European Research Council (Grant agreement no. 267864).

Appendix A: Nature of the X-ray sources

In the ACIS image we have detected 212 X-ray sources with significance >4σ. We cross matched their spatial positions with Simbad, NED, and 2MASS catalogs within a positional separation of 2″, obtaining seven matches that are listed in Table 4. All NED matches are galaxies, and the X-ray emission could be associated to the AGNs at their center. One match is the giant/sub-giant G8III/IV star (HD 10210, src # 211) with V = 8.08. The two matches in 2MASS are again two galaxies in the NED catalog.

We are left with 205 X-ray sources without matches in the above catalogs. Most of these sources are faint as shown by the cumulative distribution of the significance values (Fig. 5). The cumulative distribution has a change of slope at about $\sigma = 5$, marking the brighter sample from the rest of the sources. The number of unidentified sources with $\sigma > 5$ is 55, or the 27% of the total sample. A number of them could be distant AGNs.

For the brightest sources we did a model best fit to the spectra with one absorbed powerlaw, suited in the case of AGNs and well describing the featureless spectra that we observe in these sources. In the bright source # 64 we find a good best fit with an absorbed bremsstrahlung, but the presence of a line at ~2.5 keV is also noticed.

The G8III/IV type star HD 10210 is also detected as the brightest in the sample (source # 211), The best fit of the spectrum of HD 10210 has two temperatures at $kT = 0.37$ and $kT = 0.75$, with the cool component weighting twice the hot component in the spectrum. Overall, the spectrum is similar to that of a mid-active main sequence star, and its X-ray luminosity is $L_X \sim 1.1 \times 10^{29}$ erg/s. Detecting X-ray emission in a evolved star off of the main sequence is worth to be noticed,

References

Baliunas, S. L., Donahue, R. A., Soon, W. H., et al. 1995, ApJ, 438, 269
Bouvier, J. 2008, A&A, 489, L53
Brown, D. J. A., Cameron, A. C., Hall, C., Hebb, L., & Smalley, B. 2011, MNRAS, 415, 605
Casagrande, L., Schönrich, R., Asplund, M., et al. 2011, A&A, 530, A138
Catala, C., Donati, J.-F., Shkolnik, E., Bohlender, D., & Alecian, E. 2007, MNRAS, 374, L42
Claret, A. 2004, A&A, 424, 919
Claret, A. 2005, A&A, 440, 647
Claret, A. 2006, A&A, 453, 769
Claret, A. 2007, A&A, 467, 1389
Cuntz, M., Saar, S. H., & Musielak, Z. E. 2000, ApJ, 533, L151
Damiani, F., Maggio, A., Micela, G., & Sciortino, S. 1997a, ApJ, 483, 350
Damiani, F., Maggio, A., Micela, G., & Sciortino, S. 1997b, ApJ, 483, 370
Damiani, F., Flaccomio, E., Micela, G., et al. 2003, ApJ, 588, 1009
Delgado Mena, E., Israelian, G., González Hernández, J. I., et al. 2014, A&A, 562, A92
Deliyannis, C. P., King, J. R., Boesgaard, A. M., & Ryan, S. G. 1994, ApJ, 434, L71
Demarque, P., Woo, J.-H., Kim, Y.-C., & Yi, S. K. 2004, ApJS, 155, 667
Doyle, A. P., Smalley, B., Maxted, P. F. L., et al. 2013, MNRAS, 428, 3164
Eldridge, J. J., & Tout, C. A. 2004, MNRAS, 353, 87
Erkaev, N. V., Kulikov, Y. N., Lammer, H., et al. 2007, A&A, 472, 329
Fares, R., Donati, J.-F., Moutou, C., et al. 2010, MNRAS, 406, 409
Giardino, G., Favata, F., Pillitteri, I., et al. 2007, A&A, 475, 891
Gonzalez, G. 2008, MNRAS, 386, 928
Hellier, C., Anderson, D. R., Collier Cameron, A., et al. 2009, Nature, 460, 1098
Holmberg, J., Nordström, B., & Andersen, J. 2009, A&A, 501, 941
Houdek, G., Balmforth, N. J., Christensen-Dalsgaard, J., & Gough, D. O. 1999, A&A, 351, 582
Ip, W.-H., Kopp, A., & Hu, J.-H. 2004, ApJ, 602, L53
Israelian, G., Santos, N. C., Mayor, M., & Rebolo, R. 2004, A&A, 414, 601
Kashyap, V. L., Drake, J. J., & Saar, S. H. 2008, ApJ, 687, 1339
Knutson, H. A., Howard, A. W., & Isaacson, H. 2010, ApJ, 720, 1569
Krejčová, T., & Budaj, J. 2012, A&A, 540, A82
Melo, C., Santos, N. C., Pont, F., et al. 2006, A&A, 460, 251
Miller, B. P., Gallo, E., Wright, J. T., & Dupree, A. K. 2012, ApJ, 754, 137
Pace, G., Castro, M., Meléndez, J., Théado, S., & do Nascimento, Jr., J.-D. 2012, A&A, 541, A150
Pallavicini, R., Golub, L., Rosner, R., et al. 1981, ApJ, 248, 279
Penz, T., & Micela, G. 2008, A&A, 479, 579
Pillitteri, I., Wolk, S. J., Cohen, O., et al. 2010, ApJ, 722, 1216
Pillitteri, I., Günther, H. M., Wolk, S. J., Kashyap, V. L., & Cohen, O. 2011, ApJ, 741, L18
Pillitteri, I., Wolk, S. J., Lopez-Santiago, J., et al. 2014, ApJ, 785, 145
Pizzolato, N., Maggio, A., Micela, G., Sciortino, S., & Ventura, P. 2003, A&A, 397, 147
Pols, O. R., Schröder, K.-P., Hurley, J. R., Tout, C. A., & Eggleton, P. P. 1998, MNRAS, 298, 525
Poppenhaeger, K., & Schmitt, J. H. M. M. 2011, ApJ, 735, 59
Poppenhaeger, K., & Wolk, S. J. 2014, A&A, 565, L1
Poppenhaeger, K., Robrade, J., & Schmitt, J. H. M. M. 2010, A&A, 515, A98
Poppenhaeger, K., Schmitt, J. H. M. M., & Wolk, S. J. 2013, ApJ, 773, 62
Randich, S., & Schmitt, J. H. M. M. 1995, A&A, 298, 115
Randich, S., Singh, K. P., Simon, T., Drake, S. A., & Schmitt, J. H. M. M. 1998, A&A, 337, 372
Saar, S. H., Cuntz, M., & Shkolnik, E. 2004, in Stars as Suns : Activity, Evolution and Planets, eds. A. K. Dupree, & A. O. Benz, IAU Symp., 219, 355
Sanz-Forcada, J., Micela, G., Ribas, I., et al. 2011, A&A, 532, A6
Schröter, S., Czesla, S., Wolter, U., et al. 2011, A&A, 532, A3
Shkolnik, E., Walker, G. A. H., & Bohlender, D. A. 2003, ApJ, 597, 1092
Skumanich, A. 1972, ApJ, 171, 565
Soderblom, D. R. 2010, ARA&A, 48, 581
Southworth, J., Hinse, T. C., Dominik, M., et al. 2009, ApJ, 707, 167
Stern, R. A., Schmitt, J. H. M. M., & Kahabka, P. T. 1995, ApJ, 448, 683
Takeda, Y., Honda, S., Ohnishi, T., et al. 2013, PASJ, 65, 53
Thorburn, J. A., Hobbs, L. M., Deliyannis, C. P., & Pinsonneault, M. H. 1993, ApJ, 415, 150
Torres, G., Winn, J. N., & Holman, M. J. 2008, ApJ, 677, 1324
Trampedach, R., Asplund, M., Collet, R., Nordlund, Å., & Stein, R. F. 2013, ApJ, 769, 18
Vaughan, A. H., & Preston, G. W. 1980, PASP, 92, 385
Walker, G. A. H., Croll, B., Matthews, J. M., et al. 2008, A&A, 482, 691
Wilson, O. C. 1966, ApJ, 144, 695
Yi, S., Demarque, P., Kim, Y.-C., et al. 2001, ApJS, 136, 417

Table 2. continued.

Num.	RA (J2000) deg	Dec (J2000) deg	Pos. err arcsec	Off-axis arcmin	Significance σ_{bkg}	Counts cts	Cts err. cts	Rate ct ks^{-1}	Rate err. ct ks^{-1}	Exp. time ks
11	24.27388	–45.60273	1.3	5.93	5.34	13.81	5.74	0.183	0.076	75.59
12	24.27401	–45.62748	2	4.75	4.08	12.11	5.41	0.151	0.067	80.22
13	24.27558	–45.60022	1.5	6.02	4.12	9.84	6.11	0.131	0.081	75.09
14	24.27661	–45.64517	1.4	3.95	4.41	9.89	4.44	0.121	0.054	82.04
15	24.28193	–45.4945	9	11.83	4.02	57.15	19.28	1.872	0.632	30.52
16	24.28404	–45.64753	0.5	3.62	4.12	4.48	3.39	0.055	0.042	80.82
17	24.28427	–45.60261	1.4	5.71	4.09	9.53	4.28	0.13	0.058	73.18
18	24.28557	–45.65013	0.5	3.47	11.98	33.92	9.76	0.455	0.131	74.6
19	24.29219	–45.59813	1.1	5.8	4.25	8.3	4.95	0.115	0.069	72.25
20	24.29519	–45.57693	1.2	6.93	14.82	69.33	9.94	1.005	0.144	68.98
21	24.30081	–45.63905	0.4	3.5	4.37	5.03	2.97	0.062	0.036	81.43
22	24.3018	–45.60976	0.7	5	27.51	136.87	12.3	1.893	0.17	72.3
23	24.30209	–45.65241	0.5	2.86	4.4	5.11	4.07	0.061	0.049	83.72
24	24.30535	–45.60159	1.1	5.39	4.4	8.7	5.11	0.115	0.068	75.5
25	24.30621	–45.64441	0.6	3.1	4.73	6.6	3.93	0.082	0.049	80.17
26	24.30714	–45.64659	0.4	2.98	5.92	8.49	4.41	0.109	0.056	78.28
27	24.30823	–45.61779	0.8	4.45	4.2	6.52	4.28	0.08	0.053	81.22
28	24.31052	–45.51348	3.8	10.47	6.85	55.06	16.95	1.234	0.38	44.61
29	24.31374	–45.59013	1.4	5.94	8.09	30.25	9.07	0.414	0.124	73.03
30	24.31829	–45.66284	0.5	1.93	4.09	4.54	3.56	0.054	0.042	84.49
31	24.31834	–45.6034	1.1	5.12	4.02	7.59	4.3	0.095	0.054	79.69
32	24.3201	–45.5065	3.8	10.82	6.33	48.21	13.57	1.293	0.364	37.29
33	24.32353	–45.65841	0.6	2	8.72	20.88	7.07	0.247	0.084	84.44
34	24.32374	–45.64749	0.6	2.56	4	5.16	2.97	0.061	0.035	84.28
35	24.32418	–45.55242	2	8.07	8.91	40.28	11.74	0.613	0.179	65.74
36	24.32638	–45.64832	0.5	2.46	4.32	5.07	4.12	0.06	0.049	84.37
37	24.328	–45.57583	1.4	6.66	8.74	33.24	9.82	0.469	0.139	70.89
38	24.32838	–45.55383	2	7.96	9.18	42.02	12.16	0.67	0.194	62.74
39	24.32917	–45.63721	0.5	3.04	4.33	5.12	3.94	0.063	0.048	81.61
40	24.33661	–45.62566	0.5	3.65	4.25	4.94	3.58	0.061	0.044	80.88
41	24.33933	–45.65263	0.5	2.04	4.24	4.83	3.64	0.058	0.044	82.64
42	24.33979	–45.60188	1.4	5.05	4.06	9.43	4.37	0.118	0.055	79.83
43	24.34135	–45.64186	0.5	2.66	4.24	4.81	3.71	0.059	0.046	80.91
44	24.34422	–45.59913	1.1	5.2	4.69	9.13	4.89	0.125	0.067	73.02
45	24.34877	–45.64658	0.4	2.34	5.81	8.1	4.22	0.107	0.056	75.47
46	24.34891	–45.63556	0.5	3	4.11	4.48	3.49	0.055	0.043	81.55
47	24.35358	–45.53544	3.6	9.01	4.06	20.91	8.35	0.393	0.157	53.19
48	24.3545	–45.61487	0.9	4.25	5.88	12.79	5.04	0.157	0.062	81.47
49	24.35542	–45.64032	0.5	2.72	4.1	4.38	3.27	0.055	0.041	79.98
50	24.35714	–45.64254	0.4	2.6	4.95	5.99	4.03	0.076	0.051	78.56
51	24.3657	–45.62035	0.8	3.96	4.08	6	3.29	0.075	0.041	79.69
52	24.37347	–45.6293	0.5	3.51	4.56	5.17	4.29	0.063	0.052	81.74
53	24.37466	–45.59796	12.1	5.35	4.18	78.92	25.07	1.011	0.321	78.04
54	24.38382	–45.616	0.8	4.4	4.66	7.04	5	0.09	0.064	78.44
55	24.38498	–45.58196	1.4	6.38	4.6	10.96	5.16	0.15	0.071	72.95
56	24.38749	–45.58205	1.4	6.4	4.01	9.09	4.33	0.125	0.06	72.59
57	24.39812	–45.56449	1.1	7.53	18.76	91.19	10.84	1.53	0.182	59.59
58	24.42006	–45.58314	1.5	6.8	4.13	8.38	5.07	0.178	0.108	47.15
59	24.29277	–45.79012	3.2	6.73	5.68	27.83	9.46	0.441	0.15	63.12
60	24.2985	–45.77849	6.6	5.99	4.05	35.21	12.36	0.512	0.18	68.72
61	24.2994	–45.73798	1	3.81	9.94	31.77	9.36	0.394	0.116	80.62
62	24.30758	–45.74881	2.5	4.2	4.24	15.75	6.3	0.211	0.084	74.72
63	24.32088	–45.70922	0.5	1.9	4.1	4.35	3.45	0.052	0.041	84.03
64	24.32203	–45.7925	1.2	6.53	28.91	175	14.52	2.534	0.21	69.05
65	24.32337	–45.76748	1.1	5.05	4.15	7.41	4.21	0.097	0.055	76.07
66	24.32379	–45.72558	0.6	2.65	15.77	43.82	6.97	0.577	0.092	75.91
67	24.33132	–45.78434	1.3	5.98	10.58	33.65	6.58	0.467	0.091	72.03
68	24.33234	–45.74109	0.5	3.42	4.13	4.42	3.2	0.056	0.041	78.25
69	24.33327	–45.72204	0.5	2.31	4.53	5.19	4.29	0.064	0.053	80.89
70	24.33356	–45.72145	2.6	2.27	4.07	15.28	6.14	0.194	0.078	78.6
71	24.33479	–45.68913	0.5	0.71	4.3	5.04	3.75	0.061	0.045	83.25
72	24.33661	–45.70409	0.6	1.26	7.23	14.93	5.53	0.176	0.065	84.63
73	24.33712	–45.69782	0.8	0.93	4.1	6.32	3.32	0.074	0.039	84.92

Table 2. continued.

Num.	RA (J2000) deg	Dec (J2000) deg	Pos. err arcsec	Off-axis arcmin	Significance σ_{bkg}	Counts cts	Cts err.	Rate ct ks^{-1}	Rate err.	Exp. time ks
74	24.33959	–45.70337	0.5	1.17	4.01	4.37	3.37	0.052	0.04	84.66
75	24.34094	–45.72871	0.5	2.62	4.42	5.07	4.08	0.063	0.051	80.17
76	24.3419	–45.69908	0.6	0.89	5.57	8.69	4.59	0.102	0.054	84.89
77	24.3439	–45.80344	1.5	7.08	4.05	8.24	4.25	0.134	0.069	61.39
78	24.34441	–45.74711	0.5	3.7	4.14	4.64	3.47	0.058	0.044	79.45
79	24.34497	–45.73313	0.6	2.86	4.06	5.07	2.99	0.065	0.038	77.98
80	24.34648	–45.71	0.5	1.48	4.2	4.66	3.5	0.057	0.042	82.48
81	24.34841	–45.73554	0.6	3	8.93	21.21	6.89	0.267	0.087	79.34
82	24.34946	–45.75306	0.8	4.05	4.23	6.66	4.14	0.085	0.053	78.34
83	24.34988	–45.71375	0.6	1.69	4.24	5.39	3.08	0.066	0.038	82.02
84	24.35298	–45.70252	0.5	1.02	4.69	5.61	4.59	0.068	0.056	82.67
85	24.35363	–45.74041	0.5	3.29	4.33	4.99	3.78	0.062	0.047	80.26
86	24.35457	–45.704	0.4	1.11	4.53	5.26	3.45	0.064	0.042	81.86
87	24.35585	–45.72007	0.6	2.08	4.07	5.23	3.05	0.067	0.039	77.78
88	24.35658	–45.74429	0.5	3.53	4.36	5.12	4.08	0.064	0.051	79.57
89	24.35767	–45.72204	0.5	2.2	4.12	4.62	3.61	0.058	0.046	79.37
90	24.35804	–45.71406	0.4	1.73	20.33	65.53	8.65	0.809	0.107	80.96
91	24.36106	–45.6992	0.4	0.92	8.1	15.9	5.78	0.198	0.072	80.52
92	24.36306	–45.76098	0.9	4.55	4	6.02	4.37	0.08	0.058	75.16
93	24.36592	–45.77341	1.8	5.31	4.61	13.47	5.57	0.198	0.082	68.1
94	24.36836	–45.74684	1.1	3.75	4.01	7.29	3.76	0.092	0.048	78.89
95	24.36961	–45.75132	1.2	4.02	6.78	18.65	6.54	0.244	0.086	76.3
96	24.3703	–45.74534	0.6	3.67	4.27	5.57	3.15	0.07	0.04	79.03
97	24.37124	–45.85096	2.6	9.96	4.01	14.78	7.44	0.381	0.192	38.78
98	24.37154	–45.71299	1	1.86	4.47	8.52	3.96	0.102	0.048	83.16
99	24.3776	–45.80918	2.5	7.5	4.61	17.64	6.77	0.288	0.11	61.24
100	24.379	–45.79162	2	6.47	4.52	13.67	6.32	0.203	0.094	67.41
101	24.37945	–45.71067	0.5	1.92	4.01	4.28	3.15	0.051	0.038	83.12
102	24.3806	–45.75672	0.9	4.44	4.17	6.06	5.3	0.089	0.078	68.21
103	24.38111	–45.7741	1.1	5.46	4.01	6.66	4.24	0.113	0.072	58.72
104	24.38191	–45.78949	1.1	6.37	18.99	76.61	10.38	1.131	0.153	67.77
105	24.38656	–45.71977	0.5	2.54	14.56	43.59	7.38	0.534	0.09	81.67
106	24.38726	–45.73216	0.4	3.18	4.32	4.87	3.27	0.062	0.042	78.16
107	24.3882	–45.71446	0.5	2.33	4.63	5.43	4.56	0.066	0.055	82.16
108	24.38973	–45.79828	3.3	6.95	4.17	20.68	7.29	0.322	0.114	64.15
109	24.39143	–45.83303	2.6	9.01	4.45	16.64	7.26	0.339	0.148	49.15
110	24.39247	–45.7863	1.6	6.29	4.05	9.12	5.11	0.134	0.075	67.81
111	24.39273	–45.78776	3.3	6.37	5.09	26.61	9.37	0.398	0.14	66.93
112	24.39918	–45.76846	1.1	5.37	4.1	7.4	4.49	0.104	0.063	71.27
113	24.40015	–45.71383	0.8	2.67	8.83	23.1	7.5	0.284	0.092	81.37
114	24.40435	–45.79253	2.6	6.79	4.05	15.04	6.15	0.233	0.095	64.48
115	24.40516	–45.75647	0.9	4.82	4.01	5.61	4.07	0.075	0.055	74.44
116	24.40685	–45.7565	1	4.86	4.94	9.23	4.34	0.124	0.059	74.17
117	24.40963	–45.75314	1.2	4.74	6.99	18.56	6.82	0.249	0.092	74.44
118	24.40974	–45.77543	1.4	5.93	4.31	9.88	4.57	0.146	0.068	67.47
119	24.41799	–45.7439	0.8	4.49	4.07	5.87	3.66	0.078	0.049	74.97
120	24.41869	–45.72115	0.5	3.55	4.02	4.14	2.98	0.059	0.043	69.93
121	24.42167	–45.73172	1	4.05	10.5	33.91	9.77	0.561	0.162	60.41
122	24.42431	–45.78277	1.4	6.59	4.62	10.94	6.05	0.179	0.099	61.11
123	24.43091	–45.73349	11.7	4.41	4.34	80.19	24.62	1.105	0.339	72.55
124	24.44112	–45.80277	1.6	7.98	6.57	21.88	7.92	0.564	0.204	38.81
125	24.44278	–45.77955	1.3	6.82	4.76	11.61	5.48	0.215	0.102	53.99
126	24.46602	–45.74354	1.1	5.94	4.28	7.94	4.59	0.135	0.078	58.79
127	24.47931	–45.77024	1.9	7.4	4.39	13.54	7.43	0.396	0.217	34.2
128	24.50076	–45.75685	2.8	7.59	4.4	3.27	3.24	0.253	0.251	12.93
129	24.35544	–45.66886	0.5	1.02	6.55	11.33	4.76	0.134	0.056	84.3
130	24.36079	–45.67592	0.5	0.71	4.13	4.97	3.73	0.059	0.044	84.13
131	24.3612	–45.67118	0.5	0.97	4.08	4.68	3.65	0.056	0.043	84.26
132	24.36737	–45.6892	0.5	0.72	4.84	6.47	5.45	0.107	0.09	60.29
133	24.36739	–45.66234	0.8	1.56	4.31	6.75	3.4	0.08	0.04	84.05
134	24.37809	–45.67449	0.5	1.32	4.23	5.13	4.29	0.061	0.051	83.65
135	24.37872	–45.64912	0.4	2.48	17.34	49.91	7.37	0.597	0.088	83.61
136	24.37965	–45.68606	2.4	1.2	4.52	20.53	7.68	0.247	0.092	83.14
137	24.38679	–45.6805	0.5	1.53	4.06	4.81	3.73	0.058	0.045	83.06
138	24.38797	–45.69146	0.7	1.59	5.78	11.13	4.65	0.142	0.059	78.64

Table 2. continued.

Num.	RA (J2000) deg	Dec (J2000) deg	Pos. err arcsec	Off-axis arcmin	Significance σ_{bkg}	Counts cts	Cts err.	Rate ct ks^{-1}	Rate err.	Exp. time ks
139	24.39169	–45.68939	0.5	1.72	11.44	33.53	9.75	0.427	0.124	78.53
140	24.39241	–45.6637	0.6	2.18	4.27	5.78	3.14	0.069	0.038	83.2
141	24.39315	–45.69359	0.5	1.83	4.41	5.34	4.42	0.065	0.054	82.36
142	24.39479	–45.67303	0.5	1.99	4.11	4.74	3.6	0.057	0.043	82.85
143	24.39823	–45.68351	0.5	1.99	4.42	5.39	4.39	0.065	0.053	82.43
144	24.39822	–45.66558	0.9	2.32	5.57	12.27	5.12	0.148	0.062	82.65
145	24.40136	–45.68145	0.4	2.13	17.74	54.75	8.16	0.666	0.099	82.25
146	24.40198	–45.64646	0.6	3.18	4	5.02	2.94	0.061	0.036	82
147	24.40197	–45.63096	0.8	3.92	4.44	6.82	3.41	0.084	0.042	81.12
148	24.4051	–45.69831	0.5	2.39	4.02	4.39	3.53	0.06	0.048	72.75
149	24.4078	–45.63746	0.5	3.75	4.14	4.51	3.49	0.056	0.043	81.1
150	24.41299	–45.70784	0.8	2.92	4.09	6.26	3.46	0.079	0.044	79.51
151	24.41338	–45.66728	0.5	2.84	4.27	4.84	4.04	0.059	0.05	81.48
152	24.41502	–45.70893	0.5	3.03	4.39	5.06	4.25	0.064	0.054	79.14
153	24.41718	–45.65529	0.5	3.32	4.24	4.72	4.05	0.062	0.054	75.68
154	24.41836	–45.61015	0.8	5.34	9.28	24.55	8.35	0.32	0.109	76.75
155	24.42399	–45.67821	0.8	3.09	7.75	19.93	6.67	0.284	0.095	70.2
156	24.42602	–45.66849	0.5	3.31	4.02	4.41	3.17	0.055	0.04	80.34
157	24.42885	–45.69185	0.6	3.29	4.05	5.3	3.07	0.067	0.039	79.36
158	24.429	–45.70179	0.5	3.41	4.58	5.52	4.42	0.073	0.058	75.9
159	24.43106	–45.60423	1.4	5.93	4.41	9.97	4.48	0.136	0.061	73.23
160	24.43477	–45.71769	0.8	4.01	4.6	7.35	3.58	0.097	0.047	75.56
161	24.43754	–45.71875	1	4.14	10.96	38.71	10.96	0.516	0.146	75.05
162	24.43844	–45.7195	0.8	4.19	4.49	7.18	3.84	0.096	0.051	74.78
163	24.44013	–45.65272	1	4.23	10.32	33.19	6.53	0.422	0.083	78.71
164	24.44067	–45.71887	1.1	4.26	4.06	7.64	4.09	0.103	0.055	74.49
165	24.44059	–45.61712	1.1	5.57	4.75	8.8	4.86	0.117	0.065	75.27
166	24.44072	–45.66278	1.3	4.01	5.43	14.27	5.67	0.193	0.077	73.93
167	24.44157	–45.65206	0.8	4.3	4.07	6.43	4.24	0.082	0.054	78.53
168	24.4422	–45.6679	2.5	3.97	4.29	17.66	6.99	0.228	0.09	77.44
169	24.44296	–45.69137	0.5	3.87	4.43	5.12	3.96	0.072	0.056	70.93
170	24.44437	–45.60236	1.4	6.35	4.44	10.3	4.84	0.147	0.069	70.05
171	24.44484	–45.70421	0.9	4.09	4.09	6.03	4.78	0.081	0.064	74.17
172	24.46089	–45.72968	3.6	5.31	4	21.36	8.32	0.32	0.125	66.65
173	24.46353	–45.69563	8.8	4.76	4.23	60.95	19.95	0.821	0.269	74.26
174	24.46591	–45.63691	1.2	5.64	6.91	19.22	6.85	0.274	0.098	70.04
175	24.46607	–45.69792	1	4.88	4.79	9.73	5.62	0.133	0.077	73.41
176	24.46729	–45.60975	1.4	6.67	4.73	11.3	4.93	0.169	0.074	66.81
177	24.46935	–45.64576	0.9	5.51	12.13	35.42	6.68	0.475	0.09	74.57
178	24.47535	–45.60512	1.9	7.11	4.39	13.23	5.73	0.208	0.09	63.65
179	24.47657	–45.71793	2.4	5.61	4.7	20.28	7.5	0.325	0.12	62.41
180	24.48066	–45.6784	1	5.45	4.34	8.65	5.18	0.118	0.071	73.19
181	24.48415	–45.64896	1.8	6	4.9	15.47	6.28	0.232	0.094	66.53
182	24.4849	–45.66845	1.2	5.71	13.99	58.3	8.68	0.801	0.119	72.77
183	24.49416	–45.6706	3.4	6.07	4.47	24.56	9.05	0.346	0.128	70.97
184	24.49494	–45.65133	0.9	6.38	11.68	38.63	7.04	0.567	0.103	68.12
185	24.50131	–45.69108	1.8	6.31	4.24	14.08	5.68	0.22	0.089	63.86
186	24.50386	–45.75107	3.4	7.51	4.04	23.21	8.35	0.951	0.342	24.42
187	24.5116	–45.701	2.4	6.8	4.67	19.63	7.38	0.357	0.134	54.91
188	24.52064	–45.64591	3.5	7.5	4.4	24.91	9.49	0.391	0.149	63.74
189	24.52554	–45.61767	3.6	8.38	4.07	20.84	8.19	0.392	0.154	53.19
190	24.53792	–45.65849	1.1	8.01	16.19	83.68	10.4	1.477	0.184	56.65
191	24.59781	–45.64849	4.3	10.59	5.62	42.6	13.48	1.433	0.454	29.72
192	24.46743	–45.9031	6.2	13.93	4.37	41.86	13.72	0.727	0.238	57.56
193	24.48062	–45.90942	8.6	14.48	4.36	58.98	18.88	0.921	0.295	64.05
194	24.50558	–45.84999	8.3	11.8	4.93	62.24	19.09	1.222	0.375	50.95
195	24.51548	–45.87582	8.1	13.33	9.98	218.01	36.58	3.389	0.569	64.33
196	24.54034	–45.86973	8	13.6	5.24	68.1	20.19	0.992	0.294	68.63
197	24.55568	–45.93656	11.4	17.32	4.58	95.27	28.35	1.514	0.451	62.9
198	24.58917	–45.93872	9.9	18.16	6.01	114.43	29.8	1.851	0.482	61.82
199	24.60404	–45.86263	11.3	15	4.91	86.87	25.58	1.257	0.37	69.08
200	24.60963	–45.91614	6.5	17.56	4.01	33.94	13.87	0.543	0.222	62.47
201	24.62566	–45.96008	12	20.08	4.32	75.66	23.79	2.25	0.708	33.62
202	24.64624	–45.87741	9.8	16.89	6.84	115.51	29.76	1.782	0.459	64.83

Table 2. continued.

Num.	RA (J2000) deg	Dec (J2000) deg	Pos. err arcsec	Off-axis arcmin	Significance σ_{bkg}	Counts cts	Cts err. cts	Rate ct ks^{-1}	Rate err. ct ks^{-1}	Exp. time ks
203	24.54765	–45.80043	4	10.74	4.64	61.5	18.26	0.957	0.284	64.28
204	24.56448	–45.78471	6.3	10.74	4.22	75.39	24.99	1.081	0.358	69.72
205	24.63859	–45.79607	6.9	13.75	12.84	583.33	73.27	5.914	0.743	98.63
206	24.64888	–45.7534	8.5	13.13	4.14	121.88	38.19	1.25	0.392	97.52
207	24.65718	–45.79576	6.2	14.43	4.1	87.83	28.55	0.9	0.293	97.54
208	24.69243	–45.86424	8.3	17.86	4.21	110.11	33.98	1.413	0.436	77.91
209	24.6971	–45.75497	6	15.09	4.36	94.03	29.94	0.971	0.309	96.81
210	24.70579	–45.71968	8.7	15.01	4.04	112.33	36.64	1.171	0.382	95.91
211	24.74332	–45.7744	5.9	17.28	18.76	917.15	82.52	10.289	0.926	89.14
212	24.78107	–45.75303	9.5	18.47	8.29	233.9	58.47	2.788	0.697	83.91